Effects of Miso- and Mesoscale Obstructions on PAM Winds Obtained during Project NIMROD

T. THEODORE FUJITA AND ROGER M. WAKIMOTO

Department of the Geophysical Sciences, The University of Chicago, Chicago, IL 60637

Reprinted from JOURNAL OF APPLIED METEOROLOGY, Vol. 21, No. 6, June 1982
American Meteorological Society
Printed in U. S. A.

Reprinted from JOURNAL OF APPLIED METEOROLOGY, Vol. 21, No. 6, June 1982
American Meteorological Society
Printed in U. S. A.

Effects of Miso- and Mesoscale Obstructions on PAM Winds Obtained during Project NIMROD

T. THEODORE FUJITA AND ROGER M. WAKIMOTO

Effects of Miso- and Mesoscale Obstructions on PAM Winds Obtained during Project NIMROD

T. THEODORE FUJITA AND ROGER M. WAKIMOTO

Department of the Geophysical Sciences, The University of Chicago, Chicago, IL 60637

(Manuscript received 26 December 1981, in final form 22 February 1982)

ABSTRACT

27 PAM (Portable Automated Mesonet) stations were operated between 19 May and 1 July 1978 during the operational phase of Project NIMROD (Northern Illinois Meteorological Research On Downburst), collecting ~1 000 000 records of wind data. Analysis revealed that the PAM-measured winds are influenced by the mesoscale obstruction of the Chicago metropolitan area as a whole, as well as the misoscale obstructions of individual trees and buildings identifiable in panoramic pictures taken at each PAM site where data were being collected.

Mesoscale obstruction increased from near zero in the open field to 50% around the Chicago city limit, while the misoscale obstruction factor turned out to be as large as 58% in the wake of obstructing trees. The wind speed deficit extended 50–80 times the height of obstructing trees and buildings. The analysis of obstacle effects upon PAM-measured winds is empirical and not necessarily based upon sound hydrodynamical principles.

Misoscale and mesoscale corrections, thus derived, were applied to various situations. An example of a gust-front analysis presented in this paper shows significant differences between corrected and uncorrected wind fields, leading to the conclusion that PAM-measured winds need to be corrected for depicting the airflow free from obstacles.

1. Introduction

Since the Thunderstorm Project in the 1940s, mesometeorological networks in the United States during the 1950s and 60s were operated mostly over relatively flat terrain away from major metropolitan areas. According to Fujita's (1963) review, stations in these networks were separated by 1.6–60 km depending upon the objectives of the individual projects.

The heights of the anemometers in each network were kept constant in order to compute airflow characteristics directly from the measured winds without applying corrections for the anemometer height. In most cases, the exposures of the network anemometers were good enough to allow researchers to compute divergence, vorticity, streamfunction, and other parameters from the uncorrected winds.

Detailed analyses of uncorrected network winds were reported by Byers and Braham (1949) for the discovery of downdrafts in thunderstorms, Sanders and Paine (1975) for an intense convective storm in Oklahoma, Foote and Knight (1979) for Colorado hailstorms, Holle and Maier (1980) for downdrafts in Florida and Hobbs *et al.* (1980) for the structure of midlatitude cyclones.

Most of the network winds were recorded on strip charts, resulting in difficulties in reducing large quantities of wind data for statistical analysis. The development of PAM (Portable Automated Mesonet) by NCAR (National Center for Atmospheric Research) reported by Brock and Govind (1977) improved the usage of the network winds along with other meteorological parameters.

The PAM data are transmitted at one-minute intervals, and can be presented in map and graph forms on a real time basis. The post-network analyses of the PAM data permit us to obtain statistical aspects of the collected data, such as mean wind speeds, directional frequencies, etc.

The portable nature of PAM stations permits researchers to collect and analyze the wind data from different types of networks over non-flat terrains and in populated areas. A number of researchers used the PAM system for depicting local disturbances over various networks. Examples are: SESAME (Severe Environmental Storms and Mesoscale Experiment) network in Oklahoma by Ray *et al.* (1978), NHRE (National Hail Research Experiment) network in Colorado by Fankhauser and Mohr (1979), SPACE (South Park Area Cumulus Experiment) network in Colorado by Knupp and Cotton (1979), PHOENIX network in Colorado by Pasqualucci and Hildebrand (1980) and NIMROD (Northern Illinois Meteorological Research on Downburst) network near Chicago, Illinois by Fujita (1979).

0021-8952/82/060840-19$08.75

2. Project NIMROD network

The NIMROD network was operated between 19 May and 1 July 1978. The network, which included three Doppler radars and 27 PAM stations, was used for investigating the structure of the downburst termed by Fujita (1976) in his analysis of an aircraft accident on 24 June 1975 at the JFK Airport, New York City.

Earlier, Dyer *et al.* (1976) reported the Doppler radar signature of a severe local wind which was detected only with the lowest elevation scan. Further analyses of downbursts in relation to jet aircraft accidents by Fujita and Byers (1977) and Fujita and Caracena (1977) confirmed the existence of highly localized diverging winds which endanger the operation of aircraft at low altitudes.

The PAM stations of the NIMROD network were distributed in and around a triangle with 60 km sides located to the west of the City of Chicago (Fig. 1). The network location was chosen to include O'Hare International Airport, because one of the major objectives was to determine the low-level winds in and around major airports.

A mesoscale enlargement of the network in Fig. 2 reveals that some stations are located in the suburbs while others are in open fields. In spite of the fact that the height of all anemometers was chosen to be 4 m above the ground, it was not anticipated during the design phase of the network that the measured winds would represent the unobstructed airflow over the terrain with houses and trees in and around the large metropolitan area.

The first estimate of admittedly obstructed winds was made by computing the mean wind speed at each station. A total of 616 hours in which every single station transmitted the winds at one-minute intervals was chosen to be the statistical period. This period, equivalent to 25.7 days, is ~58% of the operational period of the network. The one-minute wind data during this period from 27 PAM stations consisted of 997 974 individual records.

The mean wind speed at each station is presented in Fig. 3 along with the isotachs drawn at 0.5 m s^{-1} intervals. As expected, but surprisingly to the authors, the mean wind speed at station 9 was 4.0 m s^{-1} which is 2.35 times the mean speed (1.7 m s^{-1}) at station 17 which was the closest (26 km) station to the Chicago Loop and No. 9 was located near the top of a small hill 71 km to the southwest of the Loop (Table 1).

If the measured winds, without any correction, were used in determining the wind field over the network, they would result in a semi-permanent pattern of divergence and/or vorticity at the anemometer height, which is related to the overall wind direction. We should not, however, make simplified corrections based on the wind-speed ratios computed from Fig. 3 because obstructions around each anemometer are not omnidirectional.

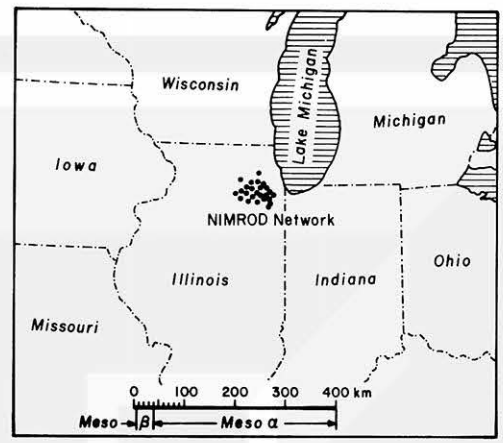

FIG. 1. The location and horizontal dimensions of the Project NIMROD network operated in 1978. A cluster of dots denotes the distribution of 27 PAM stations. For definition of meso-α (40–400 km) and meso-β (4–40 km), refer to Fujita (1981).

Owing to changes in characteristics of the boundary layer at the anemometer height, the correction factor will also be dependent upon the wind speed as well as upon the season (Frederick, 1961) and the time of the day (Bornstein and Johnson, 1977). These variations are related to the growth of trees and the instability of the atmosphere. However, a generalized correction involving these non-permanent obstructions may not be practical. To be discussed in this paper in depth are the multiple-scale wind effects related to semipermanent obstructions which may be regarded constant during the operation period of the NIMROD network.

3. Moso-, miso- and mesoscale obstructions

The generalized planetary scales defined by Fujita (1981) were used in categorizing the obstructions around anemometers, thus grouping obstructions into mososcale (0.4–40 m), misoscale (40–4000 m), and mesoscale (4–400 km) according to their distance from the anemometer. If the obstructions are uniformly distributed, the number of obstructions increases in proportion to the square of the distance.

a. Mososcale obstructions

In order to reveal the immediate environment of a PAM station, the mososcale area around each anemometer was photographed from low-flying aircraft. Examples of these aerial photographs are presented in Fig. 4. These pictures show that station No. 9 is located on the dike of a small pond to the west of the station. No. 13 is placed near the 90° bend of a road. A power-line pole is located 15 m to the east of the anemometer. No. 17 is surrounded by a

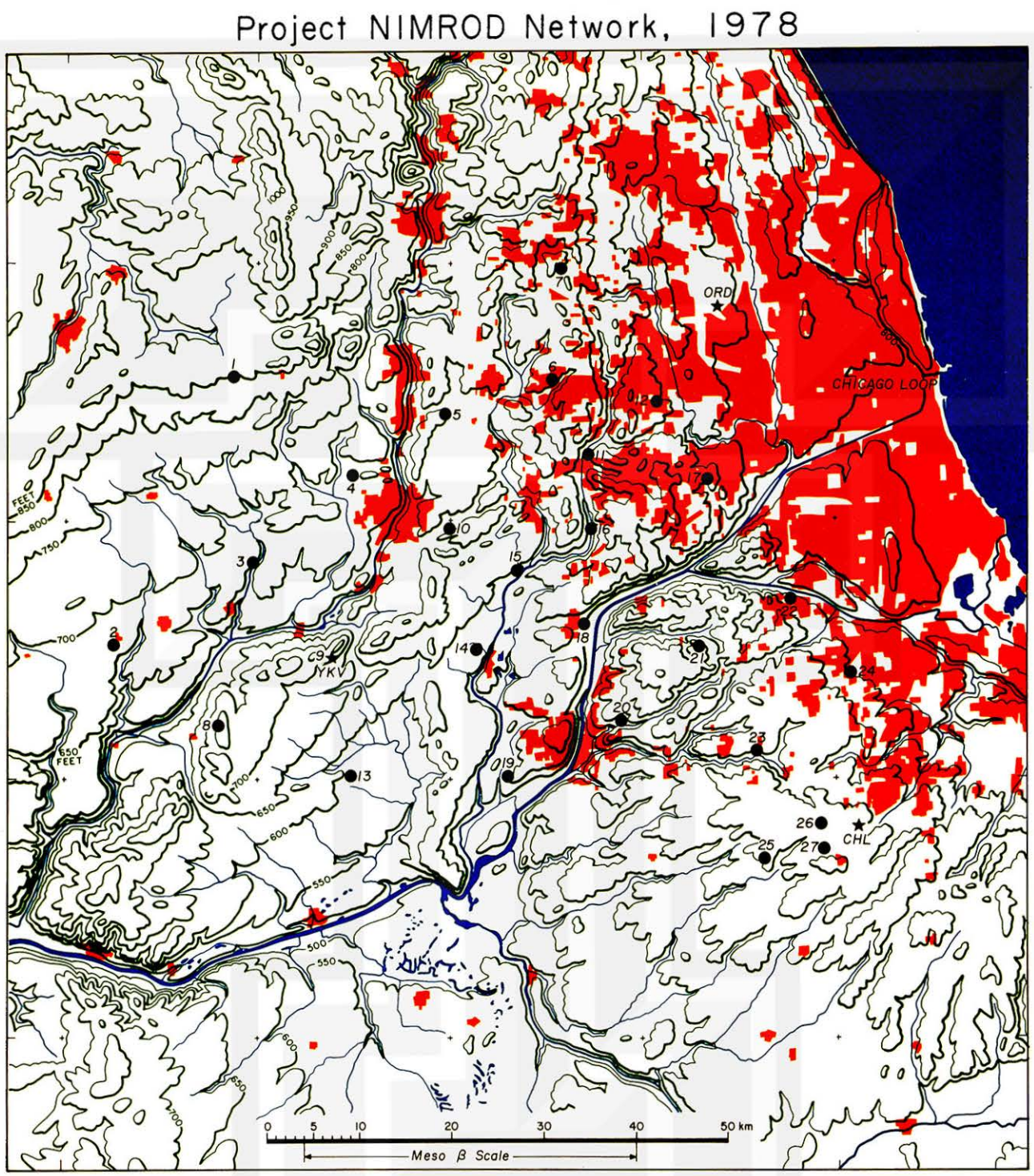

FIG. 2. Distribution of PAM stations in relation to the metropolitan area of Chicago. PAM stations are numbered 1–27 and three Doppler radars are identified by CHL (CHILL radar at Monee), YKV (NCAR's CP-3 at Yorkville), and ORD (NCAR's CP-4 at O'Hare Airport). The environmental topography is depicted by three-dimensional contour lines drawn at 50 ft intervals.

triangular fence 1 m tall. No obstruction by the fence at the anemometer height is expected to occur.

We should not underestimate the possible mososcale obstructions caused by trees and fences, however. Naegeli (1953) measured the reduction of the wind speed in the wake of obstructions of different densities. A diagram in Fig. 5 constructed from his table shows that a 2.2 m tall mat which transmits

45–55% (permeability) of the impinging airflow induces significant wind-break effects. The fractional transmission, the ratio of the measured wind speed divided by the impinging wind speed, is only 0.32 at the location 13 m behind the mat where the elevation angle of the obstruction angle in this paper is 10°. The transmission is 0.8 further down in the wake where the obstruction angle is as low as 3°.

b. *Misoscale obstructions*

The freedom to choose an anemometer site with little or no obstruction decreases with the density of the network stations. In designing the NSSP mesonet of 36 stations in Oklahoma, Fujita (1962) experienced difficulties in finding sites with little or no obstructing trees. In the end, one third of the network stations had trees with 3° or higher obstruction angles in some azimuths viewed from the anemometer.

A significant amount of time and effort was spent in searching for appropriate PAM sites in the NIMROD network, reaching the conclusion that 1–3° obstruction angles in some azimuths are inevitable for most stations.

A schematic diagram in Fig. 6 presents the obstruction angles of various terrestrial objects located within the misoscale range of an anemometer. It can be assumed that none of the network stations had obstructions within the mososcale range. Within misoscale areas, however, there may be trees and buildings with obstruction angles as large as 10°.

Obstructions within the misoscale range are usually visible above the horizon at the anemometer because the visibility under normal conditions extends far beyond the maximum misoscale range of 4 km. One could, therefore, determine qualitatively the direction and the extent of obstructions by looking 360° around the anemometer site.

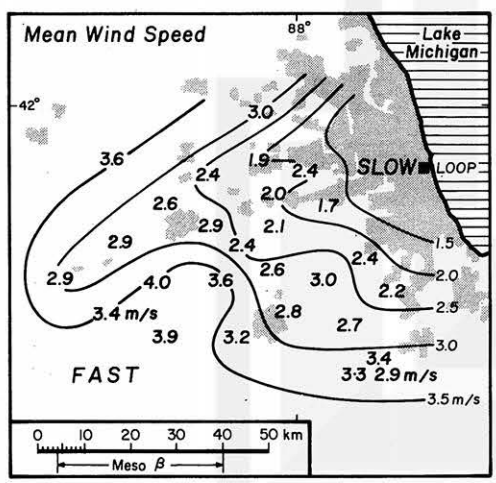

FIG. 3. 600-h mean wind speeds of 27 PAM stations showing the effects of the Chicago metropolitan area in which the mean wind speeds are significantly lower than those in the open terrain far to the west.

TABLE 1. Mean speed of 36 962 PAM winds at each of the 27 NIMROD stations used in compiling the statistics. Mean values of all winds and those excluding calm winds are tabulated, because calm winds, up to 21.2% in frequency, cannot be used in wind-direction statistics.

Station no.	Distance from Loop	Mean wind speed		Frequencies of calm	
		All winds	Excl. calm	Number	%
1	75 km	363 cm s^{-1}	378 cm s^{-1}	1365	3.7
2	93	294	310	567	1.5
3	75	293	303	2195	5.9
4	63	263	293	3548	9.6
5	53	244	262	1774	4.8
6	41	190	189	2422	6.6
7	42	297	317	2027	5.5
8	85	344	378	2022	5.5
9	71	402	429	50	0.1
10	54	287	309	380	1.0
11	38	201	216	2055	5.6
12	29	243	265	873	2.4
13	75	392	419	296	0.8
14	57	356	379	1565	4.2
15	49	237	261	2657	7.2
16	40	210	229	1166	3.2
17	26	168	171	1131	3.6
18	45	261	276	1903	5.2
19	62	316	339	789	2.1
20	49	279	294	1866	5.1
21	37	303	351	816	2.2
22	27	236	258	855	2.3
23	43	269	281	7839	21.2
24	32	215	216	888	2.4
25	54	326	346	1854	5.2
26	48	342	374	515	1.4
27	51	293	313	1955	5.3
Maximum	93	402	429	7839	21.2
Mean	52	282	302	1680	4.6
Minimum	26	168	171	50	0.1
				Total 45 373	

c. *Mesoscale obstructions*

Because of the large mesoscale range, 4–400 km, we may not be able to see obstructing objects far away from the anemometer. Distant mesoscale obstructions could result in a significant reduction of anemometer-measured winds at unexpected locations.

Central regions of large cities, such as New York City, Chicago, St. Louis, etc., along with their surrounding areas create mesoscale obstructions. An aerial photograph in Fig. 7 shows that a group of skyscrapers 200–300 m tall could cause serious obstruction effects which are not assessed in this paper. An extensive metropolitan area with relatively low

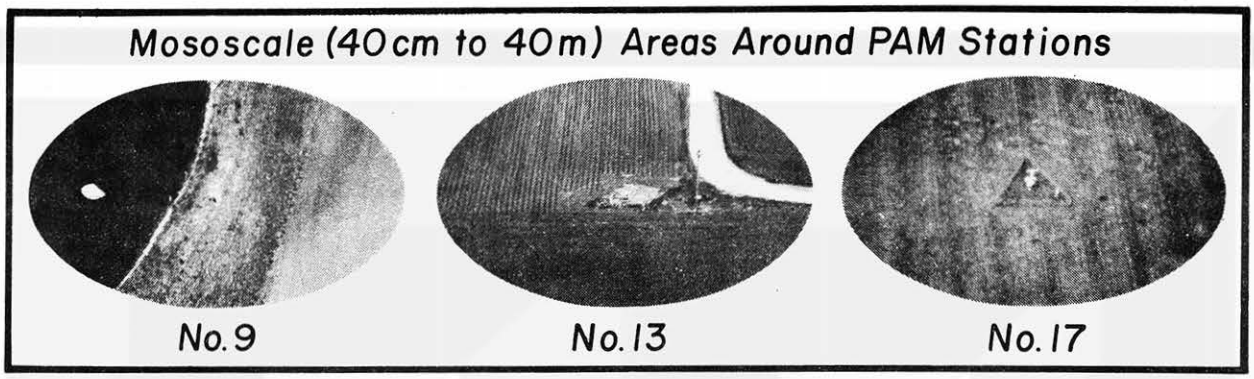

FIG. 4. Aerial photographs of circular areas within 40 m radius of PAM stations Nos. 9, 13 and 17. Similar aerial photos of all PAM stations were taken for the purpose of evaluating possible obstructions around each PAM site.

buildings and trees induces mesoscale boundary layers in which anemometer-measured winds are relatively weak.

Low mountains and small hills also create mesoscale obstructions. For example, the Ouachita Mountains between McAlester, Oklahoma and Hot Springs, Arkansas (Fig. 8) are insignificant compared with the Appalachian and Rocky Mountains but the grouping effects of these mountains could be significant enough to induce possible mesoscale obstructions which affect the airflow in southeastern Oklahoma, northwestern Arkansas, and Missouri.

d. Combined obstructions

Now we assume that U is the unobstructed, masoscale wind (see Fig. 6) blowing toward the anemometer. In the presence of multiple scale obstacles, U will be influenced by the obstructions within the mesoscale range as well as those within the misoscale range. It is the purpose of this paper to correct both miso- and mesoscale obstructions empirically in an attempt to obtain the unobstructed wind U.

The multiple-scale environment of PAM station No. 8 is presented in Fig. 9. The mososcale range is chosen to be more or less free from obstructions. However, the misoscale environment includes numerous trees which are likely to cause the reduction of wind blowing from the direction of these obstructions. The mesoscale obstructions are caused mainly by the Chicago metropolitan area located to the northeast of this station.

4. Vorticity and divergence of mean PAM winds

It has been speculated that the combined effects of miso- and mesoscale obstructions will result in both vorticity and divergence over the NIMROD network.

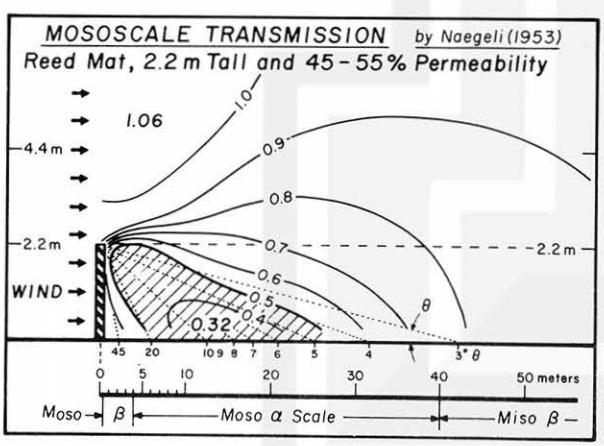

FIG. 5. Wind-break effects of a 2.2-m tall mat. The reduction of wind speed or the wind-speed deficit is seen in the wake as far as 50 m behind the mat. Based on the measured values by Naegeli (1953). This figure implies that the triangular fence, 1.2 m tall and 90% permeable, in Fig. 4 does not affect PAM winds.

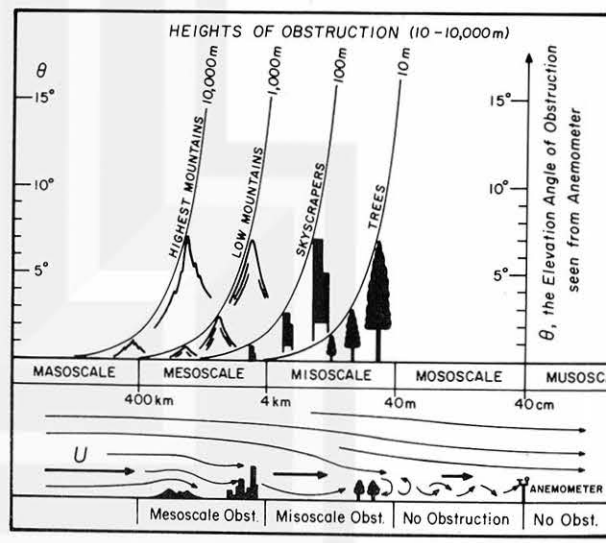

FIG. 6. Obstruction angle, the elevation angle of the obstruction seen from an anemometer, of the terrestrial objects located in the multiple-scale environment. The misoscale obstructions are caused mainly by trees and buildings while mososcale obstructions are reduced to near zero by choosing the best possible PAM site.

FIG. 7. An aerial photograph of Downtown Chicago with the metropolitan areas in the background.

An example in Fig. 10 shows a pre-storm flow on 29 May 1978 depicted by the 1-h mean PAM winds which were predominantly from the south with speeds in excess of 8 m s^{-1} at some open-field stations. In the suburbs, however, speeds were as low as 3 m s^{-1}. As expected, the relative vorticity was anticyclonic: -2×10^{-4} s^{-1}. This magnitude is approximately twice the Coriolis parameter at the latitude of the network, resulting in a negative absolute vorticity. The reduction of PAM winds toward the Chicago metropolitan area is mainly due to the mesoscale obstructions. It is most likely that the negative vorticity will disappear as the anemometer height increases.

Significant divergence (negative) is expected to occur when westerly winds blow toward the metropolitan area. The 1-h PAM winds in Fig. 11 reveal clearly the existence of a converging flow in the western suburbs where mesoscale obstructions increase toward the city. The magnitude of the maximum convergence was 8 to 10 $\times$ 10^{-5} s^{-1}. It should be noted that the wind direction turns slightly toward the left (low pressure side) as the wind speed decreases inside the zone of the maximum convergence. This is the result of an increase in the surface roughness which leads to a decrease in the wind speed as

FIG. 8. A series of steep and rolling hills in the Ouachita Mountains. Significant mesoscale obstructions are expected to occur in and around the mountains across the Oklahoma–Arkansas border.

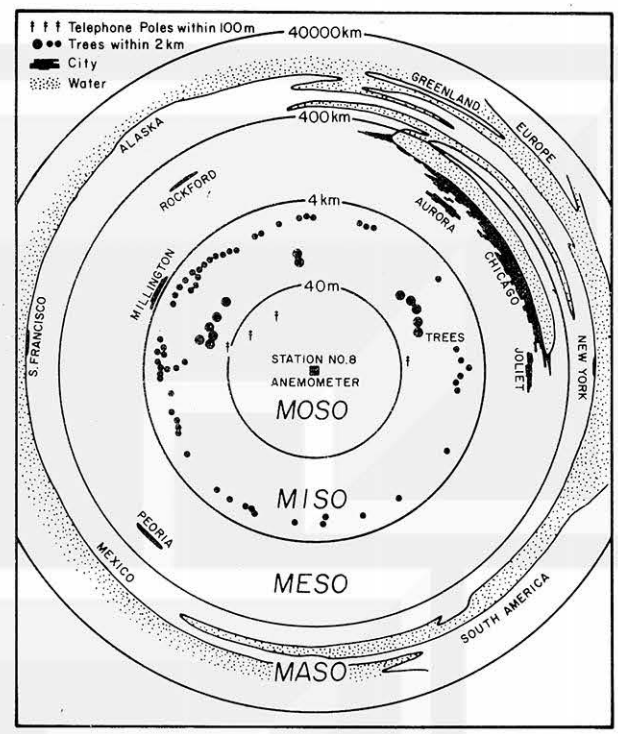

FIG. 9. The multiple-scale environment of PAM station No. 8 in the NIMROD network. There were two telephone poles inside the mososcale circle and numerous trees within the misoscale ranges. 13 trees extended above the 3° obstruction angle causing significant reduction of winds.

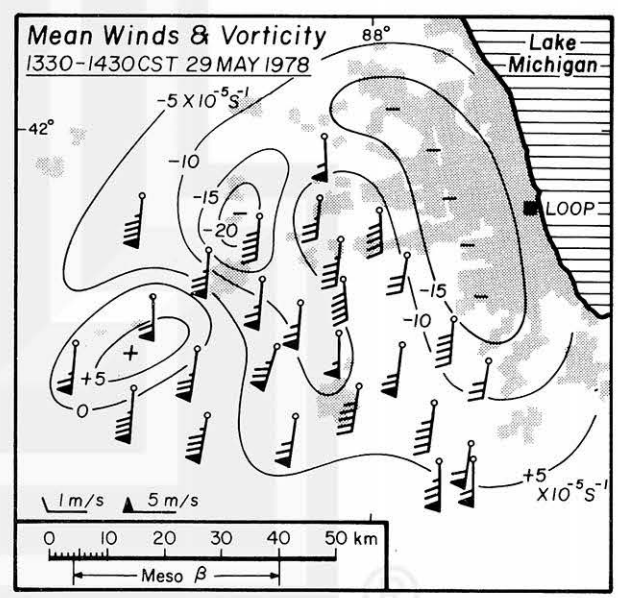

FIG. 10. Vorticity of the mean PAM winds averaged over the 1-h period between 1330 and 1430 CST 29 May 1978. Areas of negative absolute vorticity are seen in the figure.

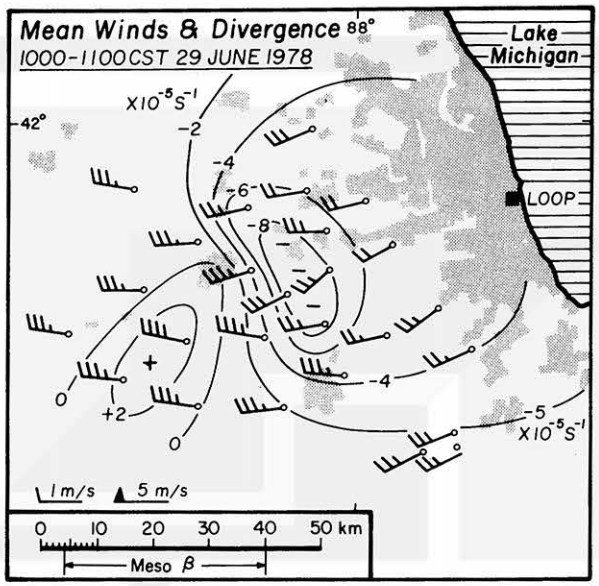

FIG. 11. Divergence of 1-h mean PAM winds. The decrease of the wind speed in the western suburbs is associated with the turning of the wind direction toward the left (low-pressure side).

well as the Coriolis force (Bornstein and Johnson, 1977).

Meteorological disturbances over the network cannot always be depicted by the winds at the height of PAM anemometers. Thunderstorm inflow, for instance, is reduced significantly when measured by PAM stations in the city. In depicting the aerial distribution of the inflow, PAM winds must be corrected taking both miso- and mesoscale obstructions into consideration. However, it should be recognized that weather system structure and evolution may indeed be responsive to subtle wind differences caused by mesoscale obstructions and terrain considerably higher than PAM stations at 4 m above the ground.

There have been studies examining the obstruction effects on wind speeds, such as by Kitaoka *et al.* (1971) and Gunn and Furmage (1976), but they did not use the results in correcting wind speeds. Wieringa (1976) discusses an objective technique to correct wind speeds without examining the anemometer environment.

5. Obstruction and transmission factors

The first step in evaluating the wind speed behind obstructions is to express the measured wind speed by

$$V = U(1 - \eta), \tag{1}$$

where V denotes the PAM-measured wind speed from a specific direction, U the unobstructed wind speed on the upwind side of the obstruction, and η the depletion of wind speed due to the obstruction. In the field of structural engineering, the product U times η is identified as the "wind-speed deficit". In this paper, we shall call η the obstruction factor.

The quantity in the parenthesis in Eq. (1) denotes the fractional transmission of the unobstructed wind speed into the wake region. It is called the transmission factor and is expressed by

$$\psi = 1 - \eta. \tag{2}$$

The horizontal scale of the unobstructed wind applicable to the NIMROD network (refer to Fig. 1) is assumed to be larger than the area of the network, blowing across the network along straight streamlines. The wind vector will change with time, being governed by the mesoscale or larger flow pattern. In other words, the unobstructed wind is expressed in the time domain as

$$U = f_1(t), \quad \delta_U = f_2(t), \tag{3}$$

where U and δ_U are the speed and direction of the unobstructed wind, respectively.

Since the PAM-measured wind is also expressed in the time domain as

$$V = f_3(t), \quad \delta_V = f_4(t), \tag{4}$$

we should theoretically be able to compute the transmission factor from

$$\psi = \frac{V}{U} = \frac{f_3(t)}{f_1(t)} \tag{5}$$

One would encounter difficulties in computing the transmission factor from Eq. (5) as a function of time, however. The two main reasons are:

1) It is not practical to determine U for the unobstructed winds at 1 min intervals, the frequency of the PAM wind.

2) The direction of the PAM wind varies from station to station while that of the unobstructed wind in Eq. (3) is assumed constant throughout the network at a given time, i.e., the transmission factor is expressed as

$$\psi = f(s, t), \tag{6}$$

where s represents the station number.

To overcome these two difficulties, a statistical analysis of the PAM wind was attempted by expressing wind speed as a function of wind direction instead of time. To accomplish this, all of the 1-min PAM wind speeds were sorted by wind direction so that the time dependence could be eliminated. We could now express V and ψ as

$$V = f_5(s, \delta), \quad \psi = f_6(s, \delta), \tag{7}$$

where δ is the direction of the PAM wind. Then the mean wind speed was defined by

$$\bar{V}(s, \delta) = \frac{1}{\Delta N} \sum_{\delta-5^\circ}^{\delta+5^\circ} V(s, \delta), \tag{8}$$

where $\bar{V}$ denotes the mean wind speed at each station averaged over a 10° azimuth, and ΔN is the

number of measurements within the 10° interval. In computing the mean wind speed, δ was chosen to be centered at the 36 point direction, δ = 0°, 10°, . . . , 360°.

The total number of PAM winds used in this statistical analysis was 952 601 which excludes calm periods. The mean ΔN per 10° wind direction per station is ~980. However, ΔN varied between 300 and 3000 owing to the direction of the prevailing wind during the data collection period and also due to the exposure of each PAM station.

a. Highest mean wind speed $\hat{V}$

For statistical purposes, the unobstructed mean wind is assumed to be the highest mean wind speed from each of the 36 point directions. Nine out of 27 network stations were characterized by the highest mean wind speeds from at least one direction. Mean wind speeds at these nine stations are shown in Table 2. The basis of this assumption is that the well-exposed station far away from the Chicago metropolitan area will measure the unobstructed wind speed for the NIMROD network. If there were no mesoscale obstructions, the station would measure the highest wind speed from any direction.

Table 2 shows that the occurrences of the highest mean wind speeds from the 36 point direction were shared by nine open-field stations instead of one. There were 12 occurrences at station No. 9, seven at No. 13, five at No. 14, four at No. 8, three at No. 25, two at No. 1 and one each at Nos. 3, 23 and 27.

b. Weighting function for smoothing azimuthal variation

In order to smooth azimuthal variations, a weighting function was applied. The function is expressed by

$$G = 1 + \cos(n\lambda) \quad -180° \leqslant n\lambda \leqslant +180°, \quad (9)$$

TABLE 2. Mean wind speed (cm s^{-1}) averaged over 10° azimuth angles of the 36-point directions at nine open-field stations with one or more occurrences of the highest wind speed $\hat{V}$ shown in the last column. The asterisk denotes $\hat{V}$.

Wind direction	Station numbers									
	1	3	8	9	13	14	23	25	27	Highest
10°	330	279	388	349	308	271	284	*457	347	*457
20°	374	340	385	396	369	275	337	*425	272	*425
30°	357	351	352	350	*440	296	321	282	232	*440
40°	286	313	182	310	*416	364	308	235	340	*416
50°	325	309	166	283	314	*417	344	254	339	*417
60°	314	233	196	276	302	294	*315	246	251	*315
70°	325	218	269	*325	312	280	293	282	251	*325
80°	344	242	*366	338	321	330	262	285	250	*366
90°	280	225	*346	314	269	265	240	229	206	*346
100°	283	195	333	*340	278	331	300	275	253	*340
110°	290	192	*344	333	268	280	274	219	277	*344
120°	280	213	*358	347	329	303	268	203	246	*358
130°	297	205	363	*390	359	288	264	296	247	*390
140°	335	222	378	*416	337	296	294	269	284	*416
150°	367	218	366	*431	347	314	317	307	277	*431
160°	446	254	432	*459	373	332	299	427	347	*459
170°	448	306	466	526	405	354	340	*546	449	*546
180°	525	378	488	*586	477	400	384	563	479	*586
190°	627	466	586	*671	604	487	428	594	507	*671
200°	576	432	596	644	*686	563	417	449	397	*686
210°	463	407	514	569	*636	594	351	368	306	*636
220°	424	410	428	431	*545	495	318	396	272	*545
230°	379	394	406	386	*451	393	311	431	237	*451
240°	440	*464	410	387	462	428	333	449	321	*464
250°	*498	483	472	399	474	467	344	380	405	*498
260°	472	389	458	424	*492	486	330	318	387	*492
270°	358	251	315	419	393	*480	250	303	287	*480
280°	324	264	269	376	368	*477	265	294	331	*477
290°	341	284	272	*392	380	383	269	318	333	*392
300°	404	311	293	*419	359	301	305	342	367	*419
310°	*434	364	364	432	376	339	324	370	405	*434
320°	383	380	350	*430	380	386	322	375	341	*430
330°	402	381	330	*423	378	362	362	324	290	*423
340°	340	360	324	365	401	*414	295	276	248	*414
350°	261	278	273	288	347	*400	260	266	182	*400
360°	255	209	274	280	279	262	230	294	*307	*307

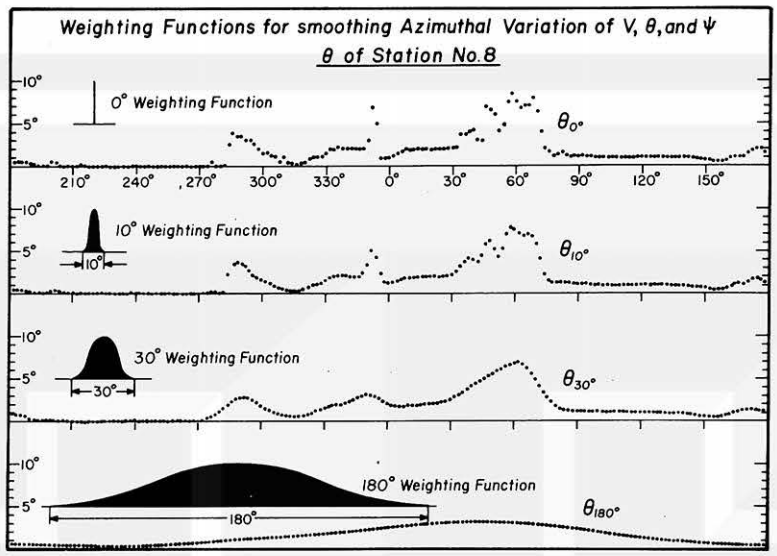

FIG. 12. Weighting functions with 0, 10, 30 and 180° azimuth width.

where λ is the angular departure on both sides of a given azimuth angle. There is no restriction in selecting a positive number n which determines the azimuthal width of G. For convenience, n is chosen to be an integer. G is equal to zero outside the angle limits in Eq. (9).

Fig. 12 shows the shape of weighting functions with their widths 0, 10, 30 and 180°. These weighting functions were applied to the obstruction angles at station No. 8. The azimuthal widths of the applied weighting functions are shown as $\theta_{10°}$, $\theta_{30°}$, etc. as suffixes to the obstruction angle θ.

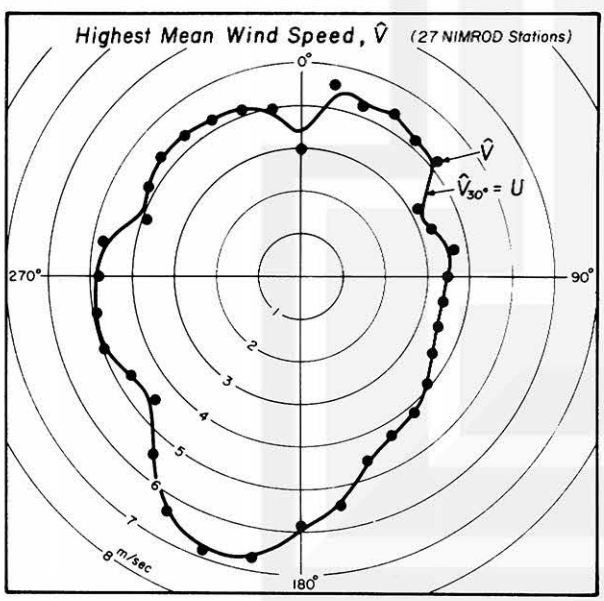

FIG. 13. Unobstructed mean wind speed U for NIMROD network defined as the 30° weighted mean values of the highest mean wind speed $\hat{V}$ from the 36-point direction.

c. *Unobstructed mean wind speed* U

The highest mean wind speeds $\hat{V}$ in the last column of Table 2 were first smoothed with 10, 20, 30 and 40° azimuth widths, finding that 30° width does not over smooth the data while suppressing unrealistic variations. Thus we defined the unobstructed mean wind speed U by

$$U = \frac{\Sigma \hat{V} G_{30°}}{\Sigma G_{30°}}, \tag{10}$$

which is a function of azimuth.

Fig. 13 shows the azimuthal distribution of $\hat{V}$ by 36 black circles. The smooth curve of U in the figure does not always pass through the black circles.

d. *Transmission factor in relation to obstruction angle*

The transmission factor ψ in Eq. (5) is defined by the ratio of PAM-measured wind speed and unobstructed wind speed at time t. Since it is not practical to estimate U as a function of time at 1-min intervals, U for the network was defined by Eq. (10) as a function of azimuth.

The PAM-measured wind speed V in Eq. (4) varies as a function of time. Eq. (7) shows, on the other hand, that it can also be expressed as a function of station and wind direction. For statistical purposes V at each station was averaged over every 1° azimuth, obtaining 360 mean wind speeds per PAM station. Then, the 10° wide weighting function G in Eq. (9) was applied in computing the smoothed wind speed $V_{10°}$ at 1° intervals of wind direction.[1]

[1] Smoothings with 5, 10, 15 and 20° widths were tested to find that 5° results in undersmoothing and 20° in oversmoothing. 15° width was the best for stations with isolated trees (station 8 in Fig. 12) while 10° width was the best for stations with forest (station 6 in Fig. 14) which require large corrections.

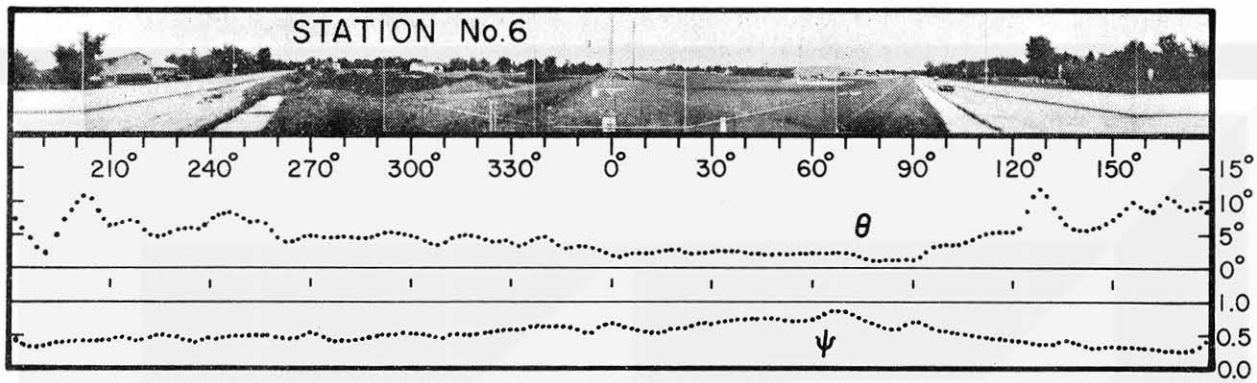

FIG. 14. Transmission factor ψ and obstruction angle θ both computed with 10° weighting of their original values at 1° azimuth intervals. Station No. 6, a suburban station.

The transmission factor $\psi_{10°}$ at a specific PAM station is defined by

$$\psi_{10°} = \frac{V_{10°}}{U}, \tag{11}$$

where U is the unobstructed wind speed from Eq. (10) which varies gradually with wind direction.

In order to smooth obstruction angles around the PAM station, the weighting function with a 10° width was applied as follows,

$$\theta_{10°} = \frac{\Sigma\, \theta G_{10°}}{\Sigma\, G_{10°}}, \tag{12}$$

where $\theta_{10°}$ denotes the obstruction angle weighted with a 10° wide weighting function.

The 10° weighting applied to both θ and ψ results in two azimuthal variations which can be correlated at each PAM station. In the rest of this paper, both $\theta_{10°}$ and $\psi_{10°}$ are written, respectively, as θ and ψ without 10° suffixes with the understanding that

$$\theta = \theta_{10°}, \quad \psi = \psi_{10°}. \tag{13}$$

Presented in Figs. 14 and 15 are azimuthal variations of θ and ψ for suburban station No. 6 and open-field station No. 8. Their variations at these stations reveal the evidence that the larger the obstruction angle the lower the wind speed. A group of trees to the south of Station 6 resulted in $\psi = 0.27$; or 73% of the wind speed from the direction of the obstruction was reduced. Only a few trees with $\theta \approx 7°$ to the northeast of station No. 8 reduced ψ to 0.49 or 51% obstruction.

Azimuthal obstructions as evidenced in Figs. 14 and 15 may occur either at open-field or at suburban stations, because they are caused by the objects located at the misoscale ranges. In other words, obstructions with a significant θ could exist around a PAM station regardless of its mesoscale environment.

6. Misoscale and mesoscale transmission factors

Scales of airflow in Fig. 6 show that the misoscale obstructions are embedded inside the mesoscale flow which is 100 times larger in horizontal dimensions. Likewise, the misoscale obstructions are 100 times larger than mososcale obstructions, if any. Thus, we express the transmission factor at a PAM site by a product

$$\psi = \psi_e \psi_i \psi_o, \tag{14}$$

where ψ denotes the measured transmission factor at the PAM station, ψ_e the transmission factor due to the objects within the mesoscale range (4–400

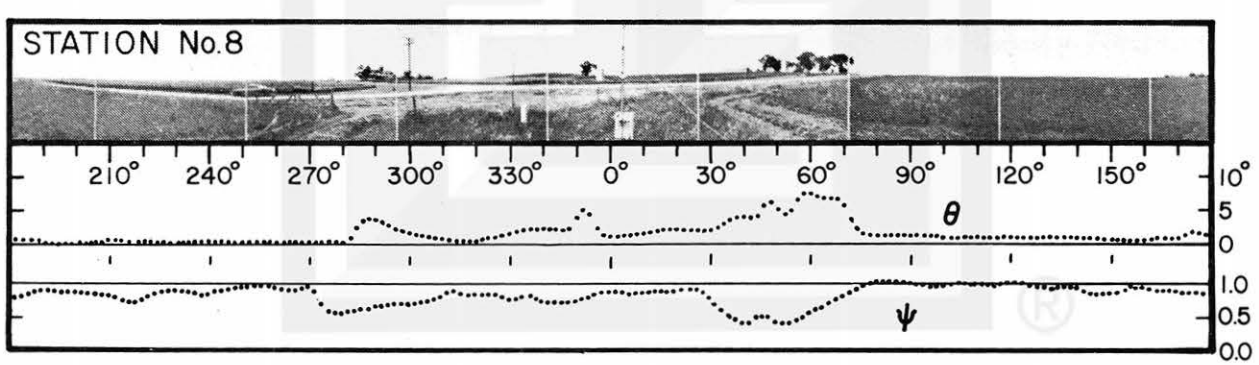

FIG. 15. ψ and θ computed with 10° weighting of their original values at 1° intervals. Station No. 8, an open-field station. Note that ψ must be shifted to the right by 7° in order to eliminate the out-of-phase between θ and ψ.

km), ψ_i that due to the objects within the misoscale range (40–4000 m) and ψ_o the mososcale (within 40 m) transmission factor which was selected to be 1.00 for all the NIMROD stations.

Eq. (14) indicates that misoscale obstructions reduce the flow speeds which were already reduced by mesoscale obstructions located on the upwind side. These mesoscale obstructions are not always visible or identifiable, because their elevation angles are very small due to their large distances from PAM stations.

On the other hand, every misoscale obstruction can be identified through panoramic and aerial photography. Their obstruction angles can be measured to 1° intervals of azimuth, for instance. It is, therefore, reasonable to estimate the misoscale transmission factor first, before attempting to determine the mesoscale transmission factor.

Windbreak effects of trees are mostly measured in a mososcale (40 cm–40 m) environment by using model trees in open fields or wind tunnels. Results of measurements have been reported by various researchers such as Iizuka (1952), Rider (1952), Naegeli (1953) and van Eimern (1964).

These measured values are variable and complicated, because not all trees are alike; tall or short, stout or flexible, top-heavy or bushy, etc. Especially when they are planted at random, in lines, or in bands, their grouping effects cannot be expressed accurately. Quantitatively and approximately, however, the taller and the denser the obstructions, the smaller the transmission factor behind the obstruction.

As the first approximation we assume that the misoscale transmission factor decreases with increasing obstruction angle, being expressed by

$$\psi_i = e^{-k\theta}, \tag{15}$$

where k is an obstruction constant (deg^{-1} unit). The misoscale transmission factor ψ_i increases to 1.00 at an infinite distance downwind where θ is zero. Most studies have shown that the misoscale transmission factor increases exponentially as the ratio of the obstruction height divided by the downwind distance increases. Since the maximum obstruction angles at PAM stations are less than 10°, the ratio can be expressed by θ instead of tanθ.

The value of k, to be estimated later in this section, turns out to be 0.0948 deg^{-1}. This constant results in the value of ψ_i at $\theta = 90°$, just behind the obstruction to be

$$\psi_i = e^{-90°k} = 0.0002 \tag{16}$$

or near zero transmission.

The closest proximity to an obstruction for a PAM station should not be where the obstruction angle is larger than 10° (refer to a panoramic picture at station No. 6 in Fig. 14). The misoscale transmission factor with $\theta = 10°$ is

$$\psi_i = e^{-10°k} = 0.39. \tag{17}$$

When we stand at a PAM station, it is hard to believe that a cluster of trees with $\theta = 10°$ (see 120–180° azimuths in Fig. 14) reduces 61% of the unobstructed wind speed impinging on the other side of the trees. Panoramic analyses of 27 PAM stations (Figs. 14 and 15 for examples), along with NCAR's calibrations, prove that these results were not caused by the instrumental errors.

The brief description of the misoscale effects of trees presented above implies strongly the need for correcting PAM-measured winds in order to depict the mesoscale airflow by suppressing or possibly eliminating misoscale obstruction effects.

a. Estimate of the misoscale transmission constant k_0 at a PAM station

A visual comparison of the azimuthal variations of θ and ψ at PAM stations No. 6 and No. 8 reveals a remarkable correspondence between these two parameters. With the exception of the well-exposed station No. 1, the linear correlation at all of the NIMROD stations was negative (Table 3).

The mesoscale transmission factor ψ_e can be obtained by dividing the measured transmission factor ψ by the misoscale transmission factor ψ_i in Eq. (15).

It should be noted that the selection of a too small k in Eq. (15) will result in an undercorrection while an excessive k, an overcorrection. The use of a proper constant, which we will call k_0, will eliminate the effects of misoscale obstructions around the PAM station, resulting in the azimuthal variation of the transmission factors which are not correlated with θ.

In order to determine k_0, the initial correlation r_i, between ψ and θ for each PAM station was computed from the conventional formula,

$$r_i = \frac{\dfrac{\Sigma \psi_j \theta_j}{360} - \dfrac{\Sigma \psi_j}{360}\dfrac{\Sigma \theta_j}{360}}{\left[\dfrac{\Sigma \psi_j^2}{360} - \left(\dfrac{\Sigma \psi_j}{360}\right)^2\right]^{1/2}\left[\dfrac{\Sigma \theta_j^2}{360} - \left(\dfrac{\Sigma \theta_j}{360}\right)^2\right]^{1/2}}, \tag{18}$$

where 360 denotes the total number of data points at each station and j designates the data points at 1° azimuth intervals, 1–360.

The initial correlation r_i computed from this equation for the PAM stations turned out to be between −0.13 and −0.80 with the exception of station No. 1 (refer to Table 3).

Although the measured transmission factor ψ is negatively correlated with θ, the correlation between θ and the ratio

$$\frac{\psi}{\psi_i} = \psi e^{+k\theta}, \tag{19}$$

TABLE 3. Obstruction characteristics of PAM stations in the NIMROD network, 1978. $\bar{\theta}$ is the mean obstruction angle averaged over 360° azimuth, $\bar{\psi}$ the mean transmission factor, r_i the initial correlation between θ and ψ, and k_0 the misoscale transmission constant with $r = 0$.

Station no.	$\bar{\theta}$ (deg)	$\bar{\psi}$	r_i	k_0 (deg^{-1})
1	1.0	0.85	positive	
2	1.8	0.67	−0.67	0.115
3	1.7	0.70	−0.39	0.115
4	1.5	0.65	−0.67	0.116
5	1.6	0.58	−0.74	0.089
6	4.7	0.48	−0.80	0.085
7	0.9	0.71	−0.26	0.048
8	1.6	0.82	−0.62	0.061
9	0.9	0.91	−0.54	0.075
10	1.0	0.66	−0.13	0.020
11	2.6	0.47	−0.60	0.131
12	1.7	0.57	−0.59	0.134
13	0.3	0.89	−0.16	0.040
14	0.4	0.84	−0.36	0.101
15	1.6	0.57	−0.36	0.058
16	3.6	0.49	−0.57	0.076
17	4.3	0.40	−0.79	0.116
18	1.4	0.62	−0.23	0.042
19	1.0	0.73	−0.52	0.111
20	1.2	0.66	−0.38	0.082
21	1.1	0.70	−0.79	0.125
22	1.0	0.54	−0.49	0.151
23	2.0	0.71	−0.62	0.112
24	3.3	0.51	−0.71	0.055
25	0.8	0.77	−0.13	0.044
26	0.7	0.78	−0.26	0.040
27	1.9	0.70	−0.16	0.024

can be brought to near zero by selecting a proper value of k. It is because ψ decreases with increasing θ while ψ_i defined by Eq. (15) also decreases with increasing θ. The rate of decrease in ψ_i can be changed by selecting different values of k.

A specific value of k which results in the zero correlation between θ and the ratio in Eq. (19) is called in this paper the misoscale transmission constant k_0.

Fig. 16 shows an example of relating θ (at the top) and ψ (at the bottom). Three variations added are three ratios computed from Eq. (19) by selecting k = 0.04, 0.08 and 0.12. It is evident that the variation with k = 0.12 is positively correlated with θ. The variation with k = 0.08 is least correlated with θ.

The increase in the correlation from negative to positive values as a function of k is presented in a diagram (Fig. 17) called the r–k diagram. For all NIMROD stations r vs. k values were computed by changing k between 0 and 0.27 at 0.01 intervals. The exact value of misoscale transmission constant k_0 was obtained by determining k at $r = 0$. Values of k_0 for NIMROD stations are presented in Table 3.

Fig. 18 was prepared to show the evidence that the larger the mean obstruction angle $\bar{\theta}$, the larger the negative value of r_i. This means that the stations with small obstruction angles should carry a lesser weight in determining k_N, the misoscale transmission constant applicable to the NIMROD network. Based on this consideration, k_N was computed from

$$k_N = \Sigma\, r_i k_0 / \Sigma\, r_i\,, \tag{20}$$

where r_i is the initial correlation between θ and ψ, and k_0 is the misoscale transmission constant for an individual station. Only r_i and $r_i k_0$ values from station No. 2 through No. 27 were used in Eq. (20) because r_i at station No. 1 was positive. The result turned out to be

$$k_N = 0.0948. \tag{21}$$

Now, the misoscale transmission factor applicable to all NIMROD stations can be computed from

$$\bar{\psi}_i = e^{-k_N\theta} = e^{-0.0948\theta}, \tag{22}$$

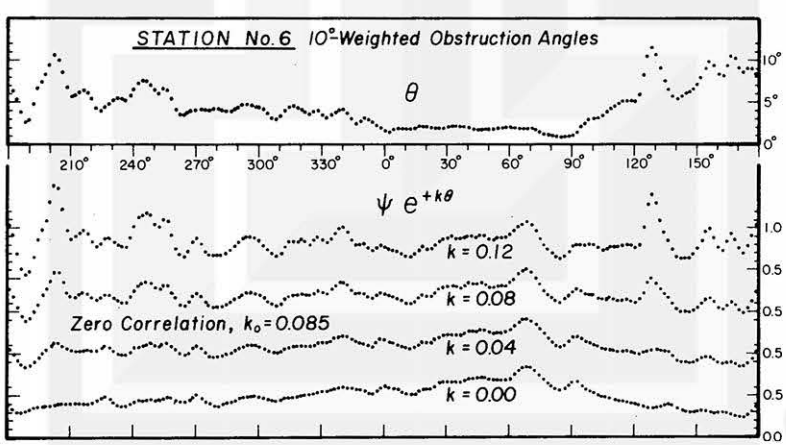

FIG. 16. Change in azimuthal variations of transmission factors at station 6 resulted by increasing the obstruction constant k. Too small k results in a negative correlation, excessive k in a positive correlation, and a correct k_0 in zero correlation.

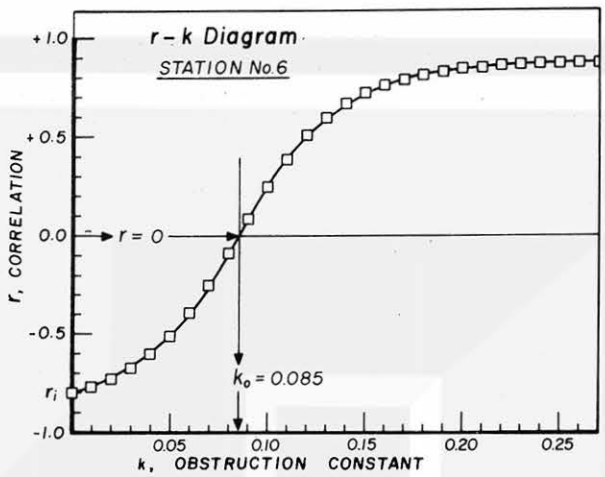

FIG. 17. Increase in the correlation r from its initial negative value r_i to positive values when k was increased in 27 steps to 0.27. Zero correlation $r = 0$ occurs with $k_0 = 0.085$ at this station No. 6.

obtained by replacing k in Eq. (15) by k_N in Eq. (21).

The misoscale transmission factors from this equation and from Naegeli's (1953) mososcale transmission experiment in Fig. 5 were combined into a diagram (Fig. 19). The vertical bars in the figure denote the range of mososcale transmission below the AGL height of the reed mat. Apparently, $\bar{\psi}_i$ for the NIMROD network is close to the lower end of the vertical bars, probably because the PAM anemometers were lower than most obstructing trees and buildings.

The good agreement between the mososcale measurement and the misoscale estimate in Fig. 19 implies that both moso- and misoscale transmission can be approximated by a function of the obstruction angle.

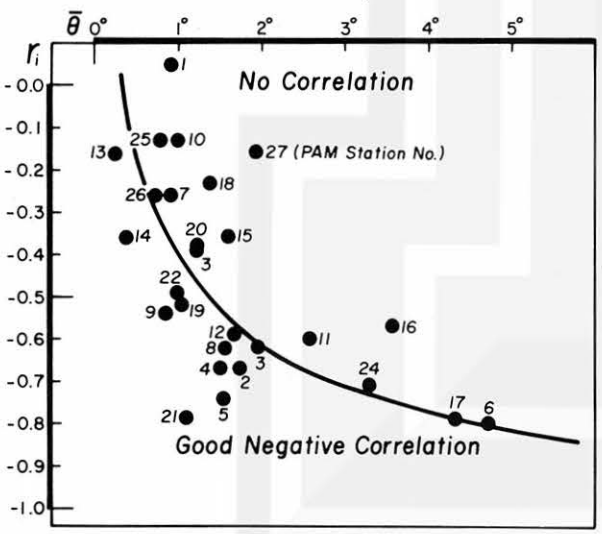

FIG. 18. Initial correlation r_i at 27 NIMROD stations plotted as a function of the mean obstruction angle $\bar{\theta}$ at each station. The negative correlation $-r_i$ increases with $\bar{\theta}$, suggesting that stations with small obstructions cannot be used in estimating the misoscale obstruction effects.

b. *Computation of mesoscale transmission factor* ψ_e

For computing the mesoscale transmission factor, we replace ψ_i in Eq. (14) by $\bar{\psi}_i$ the misoscale transmission factor applicable to all NIMROD stations. Because $\psi_o = 1.00$ for all stations, Eq. (14) can be simplified into

$$\psi = \psi_e \bar{\psi}_i , \tag{23}$$

which is written as

$$\psi_e = \psi / \bar{\psi}_i , \tag{24}$$

where ψ and $\bar{\psi}_i$ are the values computed at 1° intervals of the 360° azimuth around each station.

Evaluations of the 360° distribution of ψ_e around PAM stations showed that there are irregular variations which are not related to visible obstructions on or near the panoramic horizon. In computing the mesoscale variation of ψ_e, assumed to be relatively smooth, the weighting function of Eq. (9) with a 180° width was applied to the 360 values of ψ_e around each station. The weighted variation, to be identified as the weighted mesoscale transmission factor $\bar{\psi}_e$ is expressed by

$$\bar{\psi}_e = \Sigma\, \psi_e G_{180°} / \Sigma\, G_{180°} , \tag{25}$$

where ψ_e denotes the transmission factor from Eq. (24) within the 180° width of azimuth angles to be weighted. Table 4 presents the weighted mesoscale transmission factors at 6 NIMROD stations.

The weighted mesoscale obstruction factor expressed by

$$\bar{\eta}_e = 1 - \bar{\psi}_e , \tag{26}$$

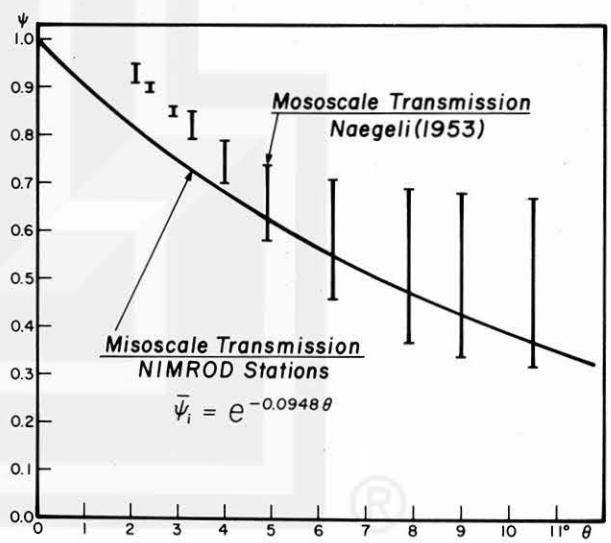

FIG. 19. A comparison of mososcale transmission measured by Naegeli (1953) and misoscale transmission for the NIMROD network estimated in this paper.

is the fractional reduction of the unobstructed wind speed due to mesoscale obstructions by cities, topography, and forests. The weighted mesoscale obstruction factor could be negative at well-exposed stations where PAM-measured winds are very high from certain directions (refer to 100% and larger factors in Table 4).

Distribution of mesoscale obstructions (%) at 27 NIMROD stations with 60 and 240° wind directions were mapped in Figs. 20 and 21, respectively. Small wind-direction dependence of mesoscale obstructions resulted from the assumption that the mesoscale wind-speed deficit (mesoscale deficit) due to the Chicago metropolitan area is insignificant at the open-field stations located up to 80 km to the southwest of the Chicago Loop. The mesoscale deficit in the wake of the city does increase the mesoscale obstructions as a function of the prevailing wind direction. Unfortunately, no wind measurements over the lake were made in assessing the mesoscale deficit across the NIMROD network.

TABLE 4. Weighted mesoscale transmission factor $\bar{\psi}_e$ (in %) at selected NIMROD stations. Values in excess of 100% are seen at the well-exposed stations at which the transmission factor ψ computed from Eq. (11) was in excess of 1.00 due to large value of V and smoothed value of U.

Wind direction	Station numbers					
	1	6	8	9	17	22
10°	91	76	97	97	65	64
20°	91	76	98	96	64	62
30°	91	77	99	96	64	60
40°	92	77	99	97	64	59
50°	92	77	100	97	63	57
60°	93	77	100	98	62	56
70°	93	76	101	99	61	54
80°	93	75	102	99	60	54
90°	93	73	102	100	59	53
100°	92	71	103	100	58	53
110°	91	68	103	100	57	53
120°	91	66	103	100	57	53
130°	90	64	103	100	56	54
140°	90	63	101	100	56	54
150°	89	63	100	99	56	55
160°	89	63	98	98	57	56
170°	90	64	95	97	57	57
180°	90	65	93	96	57	58
190°	91	67	91	95	58	58
200°	92	69	90	94	57	59
210°	92	70	89	93	57	59
220°	93	72	88	93	56	59
230°	93	73	87	93	55	59
240°	94	73	86	94	55	59
250°	95	73	85	95	55	60
260°	96	72	84	97	55	60
270°	97	72	84	99	55	61
280°	98	72	84	101	56	62
290°	98	72	85	102	57	64
300°	98	72	85	103	59	66
310°	98	72	87	103	60	67
320°	97	72	88	102	62	68
330°	96	72	90	101	63	68
340°	95	73	93	100	64	68
350°	94	74	95	99	64	67
360°	92	75	96	98	65	66

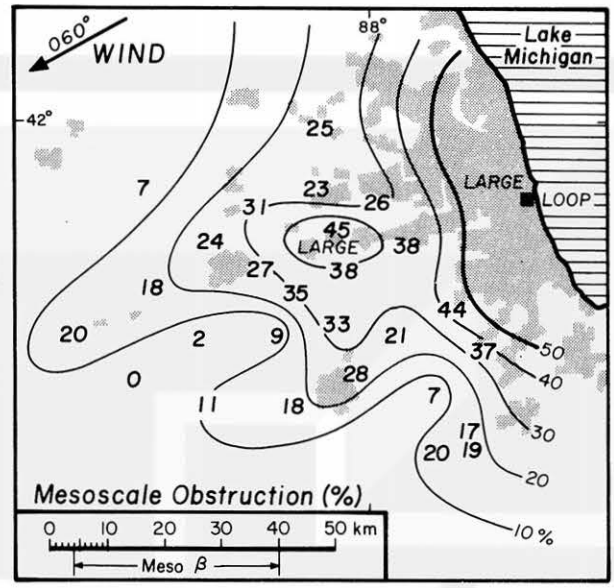

FIG. 20. Weighted mesoscale obstruction factors from Eq. (26) at 27 NIMROD stations and their isolines drawn at 10% intervals. Wind direction is 060°, from the Chicago metropolitan area to the network.

7. Wind speed corrections based on miso- and mesoscale obstructions

Foregoing analyses of wind speeds measured by PAM anemometers at 4 m above the ground revealed the reduction of the impinging winds by a number

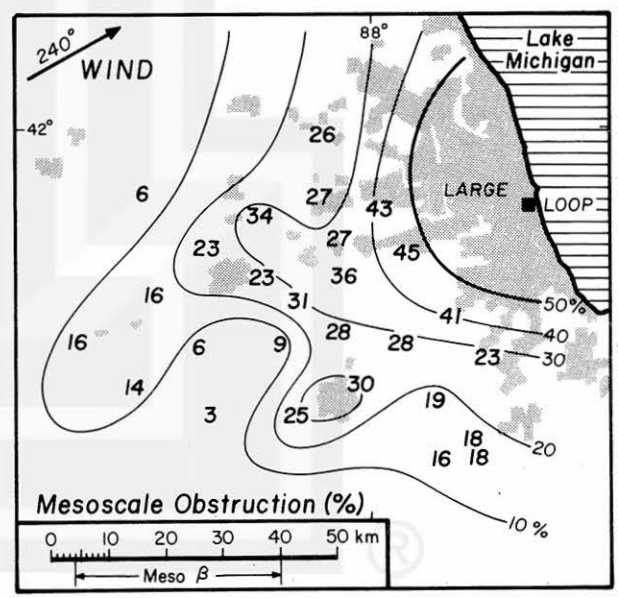

FIG. 21. As in Fig. 20 except the 240° wind direction, from the network to the Chicago metropolitan area.

FIG. 22. Streaks of high and low winds made visible by numerous corn stalks pushed over by the high winds entering the cornfield through the low spots between trees.

of obstructions inside the misoscale range (40–4000 m) and by numerous obstructions inside the mesoscale range (4–400 km).

The effect of misoscale obstructions will be insignificant above 1.5 to 2.0 times the mean height of the obstructing structures and trees. Fig. 22, for example, depicts the distribution of the corn-top (~2 m above the ground) height winds made visible by damaged stalks inside the misoscale wake of a line of trees. The corn stalks in the picture played the role of inaccurate but numerous wind indicators. Thus, a well-exposed anemometer in excess of 15–20 m height (4–5 times the PAM height) will be required in measuring the winds free from misoscale obstructions.

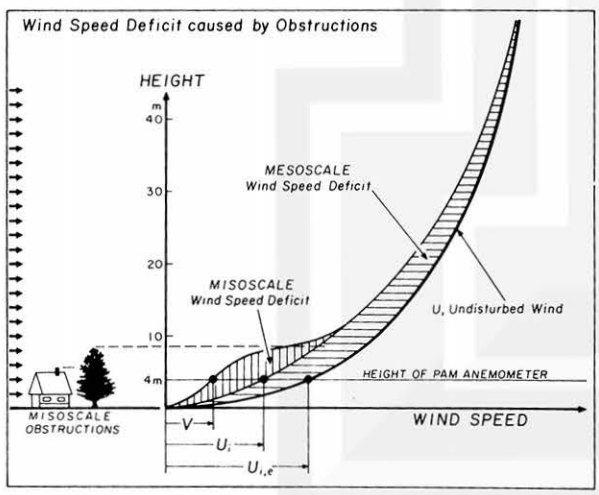

FIG. 23. Schematic diagram showing the vertical distribution of winds reduced by both miso- and mesoscale obstructions. The height of PAM stations, 4 m above the ground is too low to measure the representative wind speeds above obstruction tops.

The vertical depth of the wind-speed deficit caused by mesoscale obstructions is likely to be much deeper than that caused by misoscale obstructions. The depth will depend on the type, density, and the aerial coverage of the obstructions. It would require an anemometer at least 10 times the height of the PAM tower to measuring the wind speeds relatively free from mesoscale obstructions.

A schematic diagram of wind speeds (Fig. 23) shows the vertical distribution of the undisturbed wind U which is reduced by both miso- and mesoscale obstruction. This figure indicates that the PAM-measured wind speed V will increase to U_i after correcting the effect of misoscale obstructions and to $U_{i,e}$ after the additional correction of mesoscale obstructions. In this paper no attempt was made to estimate the wind speeds at 30, 50 m, etc. height. Nevertheless, either U_i or $U_{i,e}$ should be able to rep-

TABLE 5. Misoscale transmission factor $\bar{\psi}_i$ (in %) at selected NIMROD stations.

Wind direction	Station numbers					
	1	6	8	9	17	22
10°	91	83	84	87	75	100
20°	91	80	83	87	79	100
30°	91	80	81	87	79	91
40°	91	83	69	83	83	87
50°	91	84	61	83	83	87
60°	91	82	54	83	75	87
70°	91	83	57	87	72	87
80°	91	91	84	91	75	87
90°	91	89	89	95	79	83
100°	91	74	91	100	75	87
110°	93	64	90	100	68	87
120°	91	61	91	91	68	91
130°	91	47	91	100	65	95
140°	93	59	92	100	68	95
150°	98	50	94	100	68	100
160°	98	45	94	100	62	100
170°	96	42	88	100	51	100
180°	95	49	93	100	54	100
190°	95	58	97	100	54	95
200°	95	47	97	100	51	91
210°	91	56	99	100	59	87
220°	91	59	100	100	62	91
230°	91	59	100	100	62	91
240°	91	52	100	95	68	87
250°	91	53	100	89	65	83
260°	91	67	100	83	62	83
270°	91	65	100	83	57	87
280°	91	65	98	87	57	87
290°	91	63	79	91	57	87
300°	89	65	86	91	54	91
310°	87	70	94	91	51	91
320°	83	66	95	91	65	91
330°	87	71	87	91	75	95
340°	87	66	82	91	75	95
350°	91	75	77	91	83	95
360°	91	85	89	87	79	96

resent realistically the airflow patterns on miso-analysis or mesoanalysis maps of local disturbances.

a. Miso- and mesoscale wind-speed corrections

The misoscale transmission factor $\bar{\psi}_i$ in Eq. (22) is the ratio

$$\bar{\psi}_i = V/U_i , \tag{27}$$

where V denotes the PAM-measured wind speed and U_i the misoscale corrected wind speed.

On the other hand, the mesoscale transmission factor $\bar{\psi}_e$ in Eq. (25) is the ratio,

$$\bar{\psi}_e = U_i/U_{i,e} \tag{28}$$

where $U_{i,e}$ denote the speed of the undisturbed wind at 4 m, the height of PAM anemometers.

These equations now permit us to perform both miso- and mesoscale corrections of wind speed from

$$U_i = V\bar{\psi}_i^{-1}, \tag{29}$$

$$U_{i,e} = U_i\bar{\psi}_e^{-1} = \mathrm{V}(\bar{\psi}_i\bar{\psi}_e)^{-1}. \tag{30}$$

It should be noted that both $\bar{\psi}_i$ and $\bar{\psi}_e$ are unique values at each station, which are expressed as functions of azimuth angles at PAM tower.

Table 5 presents the values of misoscale transmission $\bar{\psi}_i$ (in %) at selected PAM stations in the NIMROD network. Values were computed from Eq. (22) by using the measured obstruction angles smoothed with a 10° wide weighting function. The largest value of 100% is seen at open-field stations with zero degree obstruction angle in some directions. No station is characterized by the 100% misoscale transmission in all panoramic directions. The smallest value of 35% is found at station No. 6 toward the 130° azimuth with the obstruction angle of a tree in excess of 10° (see Fig. 14).

The misoscale correction in Eq. (29) is performed by multiplying the measured wind speed by the inverse of the misoscale transmission factor in Table 5. For example, when the tabulated transmission is 35% the factor of $0.35^{-1} = 2.86$ was multiplied in correcting the measured wind speed.

Table 6 presents the values of miso- and mesoscale transmission factors $\bar{\psi}_i\bar{\psi}_e$ (%) in Eq. (30) at selected PAM stations in the NIMROD network. The smallest value of the combined transmission was 23%. Five stations were characterized by 33% or smaller transmission in some azimuths, corresponding to 3.00 or larger correction factors.

TABLE 6. Combined miso- and mesoscale transmission factor $\bar{\psi}_i\bar{\psi}_e$ (in %) at selected NIMROD stations.

Wind direction	Station numbers					
	1	6	8	9	17	22
10°	83	63	81	84	49	64
20°	83	61	81	84	51	62
30°	83	62	80	84	51	55
40°	83	64	68	80	53	51
50°	84	64	60	80	52	49
60°	85	63	54	81	47	48
70°	85	63	57	86	44	47
80°	85	68	86	90	45	47
90°	84	65	91	95	47	44
100°	84	62	94	100	44	46
110°	85	44	93	100	39	46
120°	82	40	94	91	39	48
130°	82	30	93	100	37	51
140°	84	37	93	100	38	52
150°	87	31	94	99	38	55
160°	87	29	91	98	35	56
170°	86	27	84	97	29	57
180°	86	32	86	96	31	58
190°	87	39	89	95	31	56
200°	87	32	87	94	30	54
210°	84	39	88	93	34	51
220°	84	42	88	93	35	54
230°	85	43	87	93	35	54
240°	86	38	86	90	38	51
250°	86	39	85	83	36	49
260°	87	48	84	80	34	50
270°	88	47	84	82	31	53
280°	89	46	83	87	32	54
290°	90	45	67	93	32	55
300°	87	46	73	93	32	60
310°	85	51	82	93	31	61
320°	80	47	84	93	40	62
330°	83	52	78	92	47	65
340°	82	48	76	91	48	65
350°	85	55	73	90	53	64
360°	84	64	86	85	51	63

b. Options of wind-speed corrections

Wind-speed corrections should not be applied blindly to all types of winds, because some disturbances are so small that their airflow may not be affected by obstructions several kilometers away from anemometer.

Option 1: No correction required. (For miso-analysis of small tornadoes, suction vortices, and microbursts, etc.) These disturbances may affect an anemometer with their airflow located on or near the ground inside the ranges of misoscale obstructions.

Option 2: Use misoscale correction only. (For mesoanalysis of urban effects, topographic influences, small mesoscale disturbances, etc.) The depiction of these disturbances requires the elimination of the wind-speed deficit at the PAM height (see Fig. 23) in the wake of misoscale obstructions, while preserving the mesoscale wind-speed deficit.

Option 3: Use miso- and mesoscale corrections. (For mesoanalysis of mesocyclones, gust fronts, etc.) The heights of the inflow and outflow of these disturbances are often much larger than those of the mesoscale wind-speed deficit, necessitating both miso- and mesoscale corrections in depicting the airflow prevailing above obstructions.

c. Correction of gust-front winds (an example)

The gust front is a mesoscale system with gusty winds pushing behind a front that extends tens of

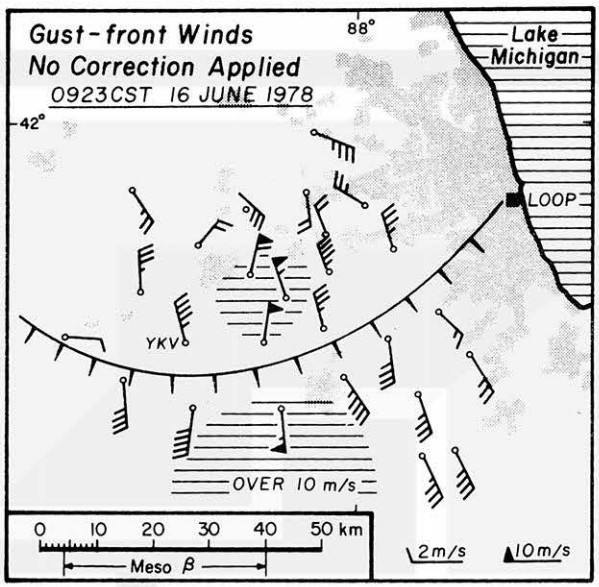

FIG. 24. Wind field of a gust front depicted by PAM-measured wind without correction. Areas of the wind speeds in excess of 10 m s^{-1} are hatched.

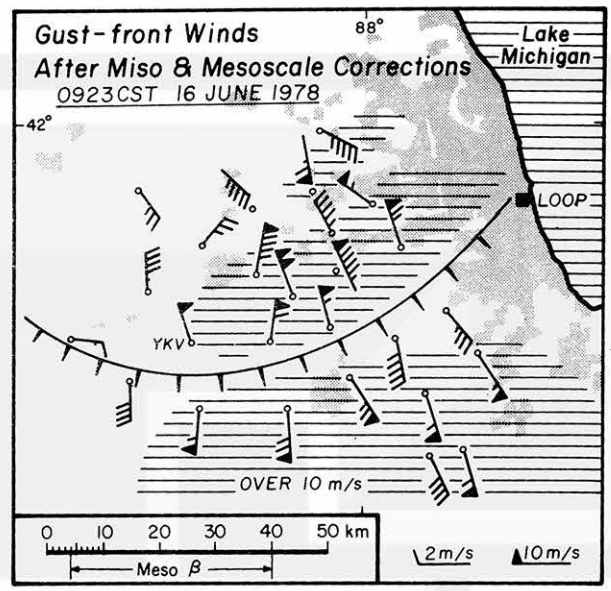

FIG. 26. Gust-front winds in Fig. 24 after miso- and mesoscale corrections by using Table 6 computed from Eq. (25). Wind speeds over the metropolitan areas increased significantly, depicting the strong push of the northwesterly winds behind the gust front.

kilometers. PAM-measured winds on both sides of the front are affected by both miso- and mesoscale obstructions.

Uncorrected PAM winds at 0923 CST 16 June 1978 appear to be fastest near the center of the network (Fig. 24). The fastest winds become more pronounced after misoscale correction in Option 2. However, the winds in the western suburbs are less than 10 m s^{-1} in spite of the fact that the strongest push of the front is expected to be there (Fig. 25).

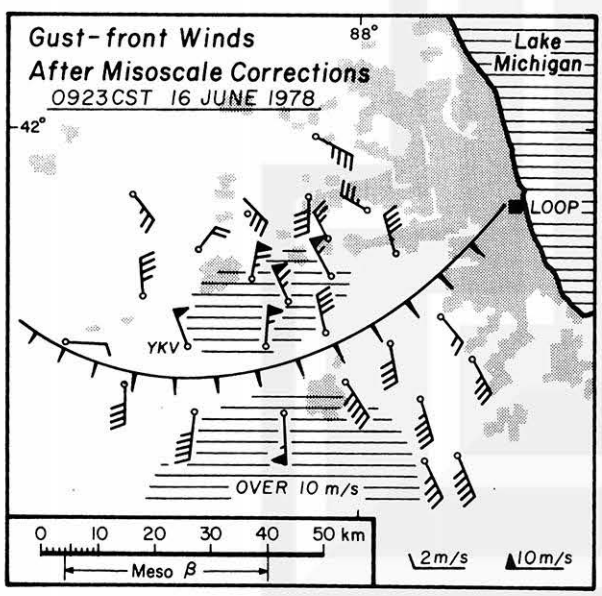

FIG. 25. Gust-front winds in Fig. 24 after misoscale corrections by using Table 5 computed from Eq. (22). Wind speeds from obstructed directions increased somewhat but the mesoscale obstruction effects still remain.

The gust-front winds after miso- and mesoscale corrections in Option 1 became in excess of 10 m s^{-1}, with the maximum speed as high as 20 m s^{-1} (Fig. 26). The 20 m s^{-1} wind speed after the correction might appear to be too high, but the Doppler-velocity analysis of the same gust front 8 min earlier by Wakimoto (1981) implies that 20 m s^{-1} wind speed is reasonable. Fig. 27 is a vertical cross-section of Doppler winds in the vertical plane along the 345° scan azimuth of the YKV Doppler radar. In spite of the fact that YKV is located where the gust front

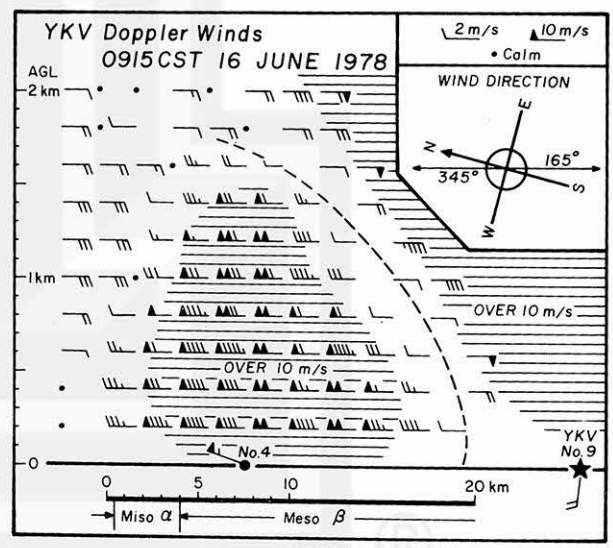

FIG. 27. Vertical cross-section of Doppler winds plotted with horizontal wind symbols in the 345° scan azimuth of the CP-3 Doppler radar at YKV. Time of the Doppler winds was 0915 CST 16 June 1978, 8 min before the map time of Figs. 24–26.

is relatively weak, 20 m s^{-1} winds were measured as low as 200 m above the ground. We may expect the existence of the 20 m s^{-1} or even higher wind speeds at the PAM station height near the center of the network.

8. Conclusions

Statistical analysis of the 997 947 PAM winds obtained during the Project NIMROD operation revealed that the measured winds were influenced by both misoscale and mesoscale obstructions, each of which can be expressed as a function of the azimuth around each station.

The mesoscale obstruction over the network area was estimated to be near zero to 50%, increasing toward the city center. On the other hand, the misoscale obstruction is closely related to nearby trees and buildings with their obstruction angles in excess 1°. Both miso- and mesoscale obstructions can be corrected with reasonable accuracies.

In spite of the one-million PAM winds used in performing the statistical analysis, transmission factors in relation to wind speed and stability could not be determined accurately. More wind data collected under extreme wind conditions will be required in performing further statistical analyses for correcting both wind direction and speed more accurately.

Acknowledgments. The authors wish to express their appreciation to the Field Observing Facility of NCAR for their successful operation of the PAM stations for Project NIMROD in 1978. The authors also wish to thank Duane J. Stiegler of the Satellite and Mesometeorology Research Project for locating and securing the PAM sites.

The research results reported in this paper were obtained under the sponsorship of NSF under Grant NSF/ATM 79-21260 and of NRC under Contract NRC 04-74-239. Meteorological aspects of this research were supported by NASA under Grant NGR 14-001-008 and by NOAA under Grant NA 80AA-D-001.

APPENDIX

List of Symbols

G	Weighting function with variable azimuth widths
$G_{10°}$	10° wide weighting function
$G_{30°}$	30° wide weighting function
$G_{180°}$	180° wide weighting function
k	Obstruction constant
k_0	Misoscale transmission constant with $r = 0$
k_N	Weighted mean k_0 applicable to NIMROD network
n	Constant which determines the width of G
ΔN	Number of wind measurements within a specific range of wind directions
r	Correlation between corrected $\psi_{10°}$ and $\theta_{10°}$
r_i	Correlation between uncorrected $\psi_{10°}$ and $\theta_{10°}$
s	Station number
t	Time
U	Unobstructed wind speed or unobstructed mean wind speed
U_i	Misoscale corrected wind speed
$U_{i,e}$	Miso- and mesoscale corrected wind speed
V	PAM-measured wind speed
$\bar{V}$	Measured wind speed averaged over 10° azimuth at each station
$\hat{V}$	Highest value of $\bar{V}$ from each 10° direction at all NIMROD stations
$V_{10°}$	Measured wind speed smoothed with 10°-wide weighting function
δ	Azimuth angle of wind direction or abbreviation of δ_V
δ_U	Direction of unobstructed wind
δ_V	Direction of measured wind
λ	Angle departure on both sides of a given azimuth
η	Obstruction factor toward a specific azimuth at each station
$\bar{\eta}_e$	Weighted mesoscale obstruction factor averaged with a 180° wide weighting function.
θ	Obstruction angles measured at 1° azimuth intervals or abbreviation of $\theta_{10°}$
$\bar{\theta}$	Mean obstruction angle at each station
$\theta_{10°}$	Obstruction angle smoothed with 10° wide weighting function
ψ	Transmission factor at 1° azimuths intervals or abbreviation of $\psi_{10°}$
$\bar{\psi}$	Mean transmission factor averaged over 360°
$\psi_{10°}$	Transmission factor smoothed with 10° wide weighting function
ψ_e	Mesoscale transmission factor from each direction at each station
ψ_i	Misoscale transmission factor from each direction at each station
ψ_o	Mososcale transmission factor from each direction at each station
$\bar{\psi}_e$	Weighted mesoscale transmission factor computed by smoothing with 180° wide weighting function
$\bar{\psi}_i$	Misoscale transmission factor for all NIMROD stations

REFERENCES

Bornstein, R. D., and D. S. Johnson, 1977: Urban–rural wind velocity differences. *Atmos. Environ.*, **11**, 597–604.

Brock, F. V., and P. K. Govind, 1977: Portable automated mesonet in operation. *J. Appl. Meteor.*, **16**, 299–310.

Byers, H. R., and R. R. Braham, Jr., 1949: *The Thunderstorm.* U.S. Govt. Print. Office, 287 pp.

Dyer, R. M., M. J. Kraus and J. F. Morrissey, 1976: Doppler observations of Auburndale windstorm of August 12, 1975. *Preprints, 17th Conf. Radar Meteor.*, Seattle, Amer. Meteor. Soc., 140–142.

Fankhauser, J. C., and C. G. Mohr, 1979: Influence of surface wind kinematics in thunderstorm evolution. *Preprints, 11th Conf. Severe Local Storms*, Kansas City, Amer. Meteor. Soc., 415–420.

Foote, G. B., and C. A. Knight, 1979: Results of a randomized hail suppression experiment in northeast Colorado. Part I: Design and conduct of the experiment. *J. Appl. Meteor.*, **18,** 1526–1537.

Frederick, R. H., 1961: A study of the effect of tree leaves on wind movement. *Mon. Wea. Rev.*, **89,** 39–44.

Fujita, T. T., 1962: Index to the NSSP surface network. NSSP Rep. No. 6, National Severe Storms Laboratory, 32 pp. [NTIS PB-168212].

——, 1963: Analytical mesometeorology; A review. *Meteor. Monogr.*, No. 27, Amer. Meteor. Soc., 77–125.

——, 1976: Spearhead echo and downburst near the approach end of a John F. Kennedy Airport runway, New York City. SMRP Res. Pap. No. 137, Dept. Geophys. Sci., The University of Chicago, 51 pp.

——, 1979: Objectives, operation, and results of Project NIMROD. *Preprints, 11th Conf. Severe Local Storms*, Kansas City, Amer. Meteor. Soc., 259–266.

——, 1981: Tornadoes and downbursts in the context of generalized planetary scales. *J. Atmos. Sci.*, **38,** 1511–1534.

——, and H. R. Byers, 1977: Spearhead echo and downburst in the crash of an airliner. *Mon. Wea. Rev.*, **105,** 129–146.

——, and F. Caracena, 1977: An analysis of three weather-related aircraft accidents. *Bull. Amer. Meteor. Soc.*, **58,** 1164–1181.

Gunn, D. M., and D. F. Furmage, 1976: The effect of topography on surface wind. *Meteor. Mag.*, **105,** 8–23.

Hobbs, P. V., T. J. Matejka, P. H. Herzegh, J. D. Locatelli and R. A. Houze, Jr., 1980: The mesoscale and microscale structure and organization of clouds and precipitation in midlatitude cyclones. I: A case study of a cold front. *J. Atmos. Sci.*, **37,** 568–596.

Holle, R. L., and M. W. Maier, 1980: Tornado formation and downdraft interaction in the FACE network. *Mon. Wea. Rev.*, **108,** 1010–1028.

Iizuka, H., 1952: On the width of windbreak. Res. Rep. No. 56, Natl. Inst. Experimental Forestry, Meguro-ku Tokyo, 231 pp. (in Japanese). [Also available from National Agricultural Library, Beltsville, MD 20705].

Kitaoka, T., S. Soma, H. Kikuchibata and M. Okuta, 1971: Regional characteristics of high winds for structural design. *Pap. Meteor. Geophys.*, **22,** 143–159.

Knupp, K. R., and W. R. Cotton, 1979: Characteristics of an intense, quasi-steady thunderstorm over mountainous terrain. *Preprints, 11th Conf. Severe Local Storms*, Kansas City, Amer. Meteor. Soc., 530–537.

Naegeli, W., 1953: Untersuchungen über die Windverhältnisse im Bereich von Schilfronhrwänden (Investigations on the wind conditions in the range of narrow walls of reed). *Mitt. Schweiz. Anst. Forstl. Versuchswes.*, **29,** 213–266.

Pasqualucci, F., and P. H. Hildebrand, 1980: Convective boundary layer thickness by in-situ and remote probes. *Preprints 19th Conf. Radar Meteorology*, Miami Beach, Amer. Meteor. Soc., 633–636.

Ray, P. S., K. K. Wagner, K. W. Johnson, J. J. Stephens, W. C. Bumgarner and E. A. Mueller, 1978: Triple-Doppler observations of a convective storm. *J. Appl. Meteor.*, **17,** 1201–1212.

Rider, N. E., 1952: The effect of a hedge on the flow of air. *Quart. J. Roy. Meteor. Soc.*, **78,** 97–101.

Sanders, F., and R. J. Paine, 1975: The structure and thermodynamics of an intense mesoscale convective storm in Oklahoma, *J. Atmos. Sci.*, **32,** 1563–1579.

van Eimern, J., 1964: Windbreaks and shelterbelts. WMO Tech. Publ. No. 70, 188 pp.

Wakimoto, R. M., 1981: Investigations of thunderstorm gust fronts from Project NIMROD data. PhD thesis, Dept. Geophys. Sci., The University of Chicago, 129 pp.

Wieringa, J., 1976: An objective exposure correction for average wind speeds measured at a sheltered location. *Quart. J. Roy. Meteor. Soc.*, **102,** 241–253.